IEEE Access
Multidisciplinary ⋮ Rapid Review ⋮ Open Access Journal

Received 17 January 2024, accepted 30 January 2024, date of publication 13 February 2024, date of current version 21 February 2024.

*Digital Object Identifier 10.1109/ACCESS.2024.3365493*

RESEARCH ARTICLE

# Short-Term Power Forecasting and Uncertainty Analysis of Wind Farm at Multiple Time Scales

**TIANREN ZHANG[1,2], YUPING HUANG[1,2,3], (Member, IEEE), HUI LIAO[1,3], XIANFU GONG[4], AND BO PENG[4]**

[1]Guangzhou Institute of Energy Conversion, Chinese Academy of Sciences, Guangzhou 510640, China
[2]School of Energy Science and Engineering, University of Science and Technology of China, Hefei 230026, China
[3]Key Laboratory of Renewable Energy, Chinese Academy of Sciences, Guangzhou 510640, China
[4]Grid Planning and Research Center, Guangdong Power Grid Company Ltd., Guangzhou 510080, China

Corresponding author: Yuping Huang (huangyp@ms.giec.ac.cn)

This work was supported in part by the Guangdong Basic and Applied Basic Research Foundation under Grant 2023A1515012372; and in part by the Science and Technology Project of China Southern Power Grid Company Ltd., under Grant 037700KK52220041 (GDKJXM20220904).

**ABSTRACT** Wind power poses a challenge to the stability of the power grid due to its unpredictability and intermittency. This study aims to analyze the forecasting law and uncertainties of short-term wind farm power forecasting (WFPF) at various time scales, in order to support the stability of energy generation. To achieve this, we propose a framework for short-term WFPF and uncertainty analysis, utilizing the whale optimization algorithm (WOA), convolutional neural network-bidirectional long short-term memory network (CNN-BiLSTM), cloud model (CM), and non-parametric kernel density estimation (NPKDE). The data is trained using a hybrid model of CNN-BiLSTM with multiple convolution and pooling methods, while the parameters are optimized using the WOA algorithm. The uncertainty of WFPF is described qualitatively by the expectation, entropy, and hyper-entropy of the cloud model, and quantified through the confidence interval based on non-parametric kernel density estimation. Test results show that the proposed WOA-CNN-BiLSTM model achieves RMSE forecasting errors of 3.79%, 4.52%, and 5.12% at 4 hours, 24 hours, and 72 hours, respectively. The maximum peak errors are less than 10.5758MW, 21.128MW, and 20.0292MW, and are better than other models. Additionally, the WOA optimization performance is superior, consistent with the results described by the cloud model. Furthermore, the RMSE forecasting value of WFPF increases with the time scale, while the growth rate of RMSE decreases with the increase of time scale. This study provides valuable insights into the uncertainties of short-term WFPF and offers a robust framework for improving the stability of energy generation.

**INDEX TERMS** Wind farm power forecasting (WFPF), uncertainty analysis, WOA-CNN-BiLSTM, non-parametric kernel density estimation (NPKDE), cloud model (CM).

## NOMENCLATURE

| | |
|---|---|
| ANN | Artificial Neural Network. |
| BELM | Bayesian Extreme Learning Machine. |
| BiLSTM | Bidirectional long short-term memory network. |
| BP | Back Propagation Neural Network. |
| CM | Cloud Model. |
| CNN | Convolutional Neural Networks. |
| CNN-BiLSTM | Convolutional Neural Network- Bidirectional Long Short-Term Memory Network. |
| CNN-LSTM | Convolutional Neural Network- Long Short-Term Memory Network. |
| ELM | Extreme Learning Machines. |
| GAN | Generative Adversarial Networks. |
| GMM | Gaussian Mixture Model. |
| GNN | Graph Neural Networks. |

The associate editor coordinating the review of this manuscript and approving it for publication was Ehab Elsayed Elattar.

| | |
|---|---|
| GWO | Grey Wolf Optimizer. |
| GWO-CNN-BiLSTM | Grey Wolf Optimization-Convolutional Neural Network-Bidirectional Long Short-Term Memory Network. |
| IPSO-LSTM-GMM | Improved Particle Swarm Optimization-Long Short-Term Memory Network-Gaussian Mixture Model. |
| IPSO-GRU | Improved Particle Swarm Optimization-Gate Recurrent Unit. |
| LSTM | Long Short-Term Memory Network. |
| MAE | Mean Absolute Error. |
| MCP | Multi-Convolution and Multi-Pooling. |
| NWP | Numerical Weather Forecasting. |
| PSO | Particle Swarm Optimization. |
| PSO-BP | Particle Swarm Optimization Back Propagation Neural Network. |
| PSO-CNN-BiLSTM | Particle Swarm Optimization-Convolutional Neural Network-Bidirectional Long Short-Term Memory Network. |
| RMSE | Root Mean Square Error. |
| SC | Single-Convolution. |
| SCSP | Single-Convolution and Single-Pooling. |
| SCMP | Single-Convolution and Multi-Pooling. |
| SD | Standard Deviation. |
| SGM | Single Gaussian Model. |
| TCN | Temporal Convolutional Network. |
| VMD-ELM | Variational mode decomposition- Extreme Learning Machines. |
| WFPF | Wind farm power forecasting. |
| WNN | Wind farm power forecasting. |
| WOA | Wind farm power forecasting. |
| WOA-CNN-BiLSTM | Whale Optimization Algorithm-Convolutional Neural Network-Bidirectional Long Short-Term Memory Network. |
| WOA-QRCNN-BiLSTM | Quasi recurrent-Convolutional Neural Network-Bidirectional Long Short-Term Memory. |

## I. INTRODUCTION

Wind energy is a rapidly expanding sustainable and eco-friendly power source, with an annual installation of over 50 GW of new wind power globally [1]. However, the unpredictable and intermittent nature of wind power presents significant challenges for large-scale grid integration, impacting the safe and cost-effective operation of the power grid. The power output of each wind turbine is influenced by various factors, including wind speed, wind direction, temperature, and humidity, making it challenging to accurately predict the power output of an entire wind farm solely by forecasting individual turbine outputs. Predicting the power output of the entire wind farm allows for the comprehensive consideration of multiple turbine influencing factors. Through scientific data analysis and model forecasting, a more precise forecast of the overall power output of the wind farm can be achieved, providing a reliable basis for the operation and management of the wind farm. Wind farm power forecasting (WFPF) technology has emerged as an effective solution to mitigate the adverse impacts of wind power generation on the grid and enhance wind power integration. WFPF provides crucial technical support for ensuring the safety, stability, and economic viability of power systems and wind farms..

In the current research field of wind power forecasting, the forecasting time scale can be divided into medium-and-long term forecasting, short-term forecasting, and ultra-short term forecasting [2], [3], [4]. From the perspective of forecasting theory, WFPF studies can be separated by physical and statistical forecasting methods [5], [6], [7]. Due to the instability and nonlinearity of WFPF, traditional data-driven forecasting methods can produce significant deviations. The use of deep learning-based forecasting models has shown stronger nonlinear fitting ability and improved accuracy in wind power forecasting [8]. Previous studies have proposed various deep learning algorithms for WPF, including LSTM, ANN, TCN, GAN, and GNN [9], [10], [11], [12], [13], [14]. These methods have established a solid foundation for improving WFPF forecasting accuracy [15], [16]. However, there is still a lack of in-depth research on the forecasting characteristics of wind power at different scales and the analysis of forecasting errors in wind power. Therefore, this study proposes a novel wind power forecasting and uncertainty analysis framework based on WOA, CNN-BiLSTM, CM, and NPKDE to analyze the uncertainties of WFPF at different short-term scales.

In addition, the development of wind power forecasting models has evolved from single forecasting models to hybrid forecasting models [17], [18], [19]. In the realm of deep learning hybrid model research, Reference [20] proposed the use of the VMD-ELM hybrid algorithm for short-term wind power forecasting, demonstrating a significant improvement in forecasting accuracy compared to the single ELM algorithm. Similarly, Reference [21] introduced a hybrid forecast based on ARIMA-GARCH-T, which exhibited enhanced forecast performance compared to a single model. Notably,

successful attempts have been made with the CNN-LSTM algorithm. For instance, Reference [22] developed a hybrid model based on CNN and LSTM for ultra-short-term wind power forecasting, resulting in a 10.97% increase in accuracy. However, the stability and adaptability of short-term forecasting at different time scales in wind farms require further verification. Additionally, most WPF studies predominantly rely on wind speed time series data, with limited consideration of numerical weather forecasting (NWP) data and the optimization of model parameters.

In the domain of wind power forecasting uncertainty analysis, accurate uncertainty analysis is crucial for maintaining power supply-demand balance and reducing the rotating spare capacity of power generation units [23], [24]. Current uncertainty analysis in power forecasting primarily focuses on two methods. The parametric method involves using historical single point forecasting errors as input for the model based on a single point forecasting model [25], [26]. On the other hand, the non-parametric method employs non-parametric estimation to enhance the theory of the conditional distribution of WFPF errors, typically constructing uncertainty confidence intervals using distribution laws [27]. Reference [28] utilized the Gaussian distribution to analyze wind power uncertainty, while Reference [29] proposed a probabilistic forecasting analysis of wind power based on improved kernel density estimation and established confidence intervals. To enhance the precision of rolling bearing remaining life predictions, Song et al. introduced an innovative heavy-tailed degradation model with power drift [30]. This model accounts for the long-range dependencies in degradation patterns and leverages fractional stable motion for diffusion modeling. Additionally, they applied variational mode decomposition to effectively discern degradation trends from noisy vibration signals, significantly improving forecasting accuracy.

Despite significant advancements in wind power forecasting uncertainty analysis methods, most studies concentrate on the quantitative analysis of wind power forecasting results [31], assuming the wind power error distribution as a single-model distribution by parameter estimation. However, the uncertainty of wind power forecasting is characterized by irregular fluctuation and chaos, necessitating qualitative analysis prior to quantitative analysis. While the application of cloud theory has been extended to uncertainty evaluation and qualitative analysis [32], [33], limited discussions exist in the context of WFPF in depth.

As shown in TABLE 1, although existing research has delved into wind power forecasting and its uncertainty analysis, further exploration is warranted to characterize multi-scale wind power forecasting and uncertainty analysis. For this, this study proposes to construct a comprehensive WFPF framework incorporating WOA, CNN, BiLSTM, Cloud Model, and non-parametric kernel density estimation, referred to as WOA-CNN-BiLSTM-CM-NPKDE, facilitating WFPF and uncertainty analysis under different time scales. The combination of CNN-BiLSTM leverages the advantages of CNN and BiLSTM to extract potential features among continuous sequences, addressing the deficiency of long sequence information and making it suitable for learning long time scale data and multi-dimensional feature data. Furthermore, the WOA group intelligent optimization algorithm is integrated to further optimize the learning parameters of the CNN-BiLSTM model. In addition, the CM-NPKDE is applied for qualitative and quantitative analysis of forecasting, redefining the performance of WFPF in uncertainty through evaluation indicators such as expectation, entropy, and hyper-entropy. The non-parametric kernel density estimation is adopted to further analyze the WFPF based on the cloud model, clarifying the uncertainty patterns caused by WFPF across different time scales.

This study aims to provide valuable insights into the uncertainties of short-term WFPF and offer a robust framework for improving the stability of energy generation. The main contributions of this study are summarized as follows.

1) Development of a comprehensive forecasting framework, the WOA-CNN-BiLSTM-CM-NPKDE model, which addresses the limitations of quantitative forecasting and standardizes the workflow of WFPF uncertainty analysis. In comparison to existing forecasting algorithms and uncertainty analysis models, this framework enables both qualitative and quantitative evaluations of multi-time scale WFPF models, leading to improved stability and accuracy of forecasting results.

2) Exploration of forecasting and uncertainty patterns of wind farms at different time scales, providing valuable data and theoretical insights for the accurate forecasting of wind farm power in the future.

The structure of the remainder of this paper is organized as follows. Section II describes the WOA-CNN-BiLSTM network and model construction. Section III introduces the CM-NPKDE methodology for uncertainty analysis. Section IV presents a comparative analysis of multiple time-scale model forecasting results and discusses the uncertainty analysis of WFPF. Finally, Section V concludes this study.

The structure of the remainder of this paper is organized as follows: Section II describes the WOA-CNN-BiLSTM network and model construction. Section III introduces the CM-NPKDE methodology for uncertainty analysis. Section IV presents a comparative analysis of multiple time-scale model forecasting results and discusses the uncertainty analysis of WFPF. Finally, Section V concludes this study.

## II. WOA-CNN-BILSTM MODEL

### A. STRUCTURE OF CNN

A CNN has multiple filters essentially and is capable of extracting spatial features hidden in data [34]. The number of convolutional and pooling layers can impact the richness of the extracted features, which affects the data analysis results of a learning model. For this reason, this study aims to improve the CNN structure with convolutional and pooling layers.

**TABLE 1. Model superiority and function.**

| Attribute | Model | Superiority | Function |
|---|---|---|---|
| Single model | LSTM[9] | Extract latent features between consecutive sequences | Improved the accuracy of short-term WPF |
| Hybrid model | VMD-ELM [20] | Decompose the feature data and improve the feature extraction ability | Improved the accuracy of a small range of wind electric power |
| | ARIMA-GARCH-T[21] | Capture the spatial and temporal correlation of multiple wind farms | The scenario power forecasting method of multiple wind farms is built. |
| | CNN-LSTM[22] | Extract latent features between consecutive sequences addresses the lack of information on long sequences, making it suitable for learning long timescale data and multidimensional feature data | Improve the accuracy of ultra-short-term wind power forecasting |
| Parameterize method | GMM[28] | Many natural phenomena and measured data follow a Gaussian distribution | We prove that the wind power distribution tends to be normal distribution |
| Non-parametric method | Kernel density estimation[29] | It can be adapted to different data features by choosing different kernel functions and bandwidth parameters, with good flexibility. | It can show the state of the wind power forecasting very well, and the confidence interval is established according to the distribution. |

In this study, multi-layer convolution kernel is added to the traditional single convolution operation, and features are extracted from the input matrix from different angles many times. This can generate multiple feature graphs, allowing that the feature information become more abstract and complete. Meanwhile, the multi-pooling technology of max-pooling is added in this study on the basis of multi-layer convolution. The feature points can be sampled in the convolutional feature graph by pooling technique to obtain new features. Compared with traditional single pooling and no pooling techniques, more topic features can be extracted, potential valid information is prevented from being lost in a single pool, and the overfitting risk is lowered [35]. The MCP structure in CNN is shown in Fig. 2

To facilitate convolution and reduce computational work, the width of $K$ convolution kernel is set as $m$ and the convolution scale is set as $f$. The convolution formulas are defined as follows:

$$c_i = T(\left[x_i : x_{i+f-1}\right] \times K_i + b_i) \tag{1}$$

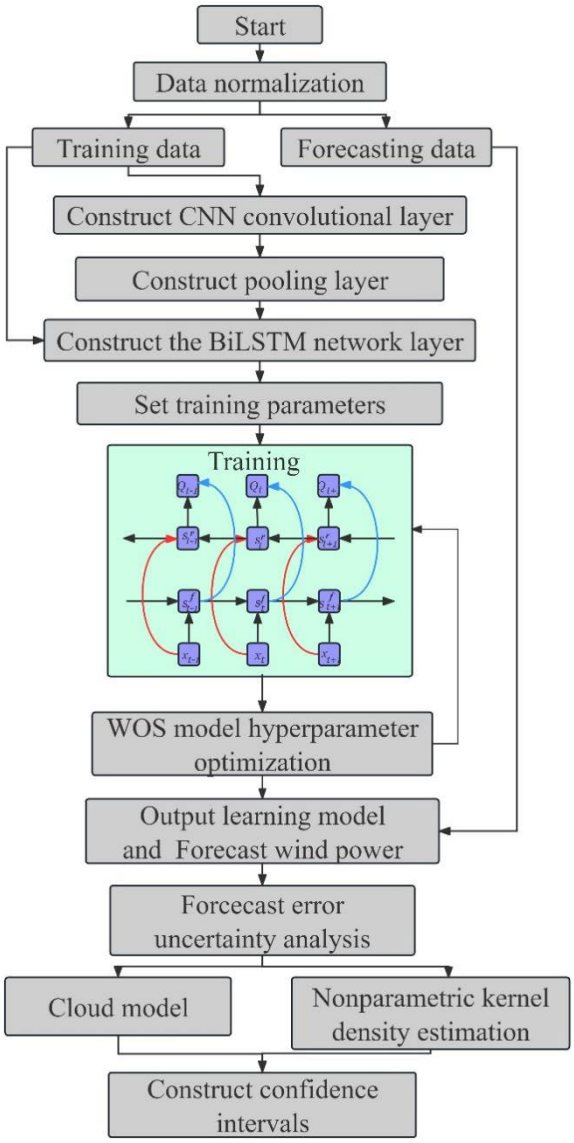


**FIGURE 1. The flowchart of short-term WFPF and uncertainty analysis based on the WOS-CNN-BiLSTM-CM-NPKDE model.**

$$C = [c_1, c_2, \ldots, c_{i+f-1}] \tag{2}$$

where $T$ is the activation function; $\left[x_i : x_{i+f-1}\right]$ is the $i$ to $i+f-1$ matrix vectors in $X$; $b_i$ is offset.

In the process of the error gradient computation, gradient explosion may occur when the computational size becomes large. Here, it incorporates a rectified linear unit (ReLU) function into the convolution process. Unlike other activation functions, such as sigmoid, it can avoid suffering from saturation problems and increase the sparsity of the network during the convolution process, better to solve the gradient explosion problem. The calculation formula is as follows.

$$ReLU(x) = max(0, 1) \tag{3}$$

### B. MODEL STRUCTURE OF BiLSTM

Temporal data exist, having a correlation with the previous data and extending to the subsequent data. Although LSTM

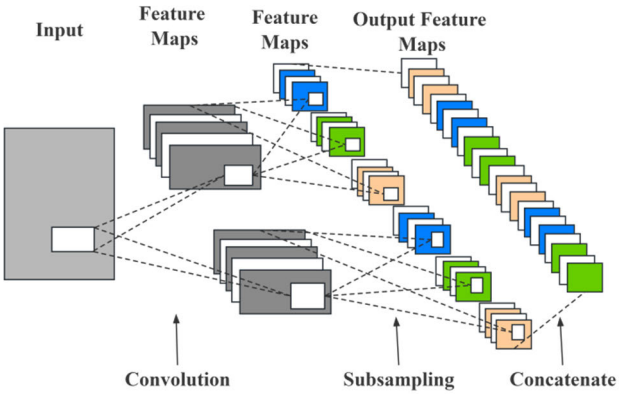


**FIGURE 2.** CNN multi-convolution and multi-pooling structure diagram.

models are able to perform forward data feature extraction on temporal data, they are not able to perform backward data feature extraction. As a variant structure of LSTM, BiLSTM can perform bidirectional feature extraction because it contains both forward and backward propagation layers.

Fig. 3 shows the BiLSTM model, in which each unit state contains two hidden layers—-forward LSTM layer $s_t^f$ and reverse LSTM layer $s_t^r$. By using these layers, the past information and the future information of the input sequence can be respectively obtained, and then the state of the two hidden layers can be connected to obtain the same output $Q_t$. Its computation is shown in (4)-(6).

$$s_t^f = \sigma\left(W_{xs^f} x_t + W_{s^f s^f} s_{t-1}^f + b_{s^f}\right) \tag{4}$$

$$s_t^r = \sigma\left(W_{xs^f} x_t + W_{s^r s^r} s_{t+1}^r + b_{s^r}\right) \tag{5}$$

$$Q_t = W_{s^f Q} s_t^f + W_{s^r Q} s_t^r + b^Q \tag{6}$$

where $\sigma$ is the activation function; $b$ is the corresponding bias vector; $W_{xs^f}$, $W_{s^f s^f}$ and $W_{s^f Q}$ are the weight matrices of the input layer, the hidden layer, and the output layer, respectively.

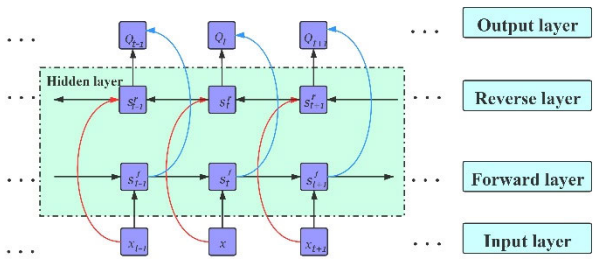


**FIGURE 3.** BiLSTM network model structure.

### C. CNN-BiLSTM STRUCTURE BUILDING

Although CNNs specialize in extracting the features of data, they only consider the correlation linkage of adjacent vectors of data, and they fail to cover the temporal order between continuous data. Although BiLSTM models can deal with time-series-related features, their feature extraction is not as comprehensive as that of CNNs. This study thus integrates a CNN and a BiLSTM to form a new hybrid model with the ability of CNN to extract unique features and the ability of BiLSTM to solve the problem of temporal features. The structure of the CNN-BiLSTM hybrid model is displayed in Fig. 4.

The layers of the CNN-BiLSTM model are as follows.

1) Input layer: The training data are passed into the model.

2) Sequence folding layer: The time step of the image sequence can be independently convoluted by using the sequence folding layer.

3) Convolution layer: This layer performs the convolution calculation on the input by using filters that move vertically and horizontally along the input direction, counting the convolution of the weights with the input, and finally adding a deviation term.

4) Multi-scale maximum pooling layer: The maximum pooling layer performs sampling by dividing the input into rectangular pooling regions and calculating the maximum value of each region.

5) ReLU layer: The interdependence between the parameters is reduced, the overfitting problem is relieved, and the gradient dissipation problem is solved.

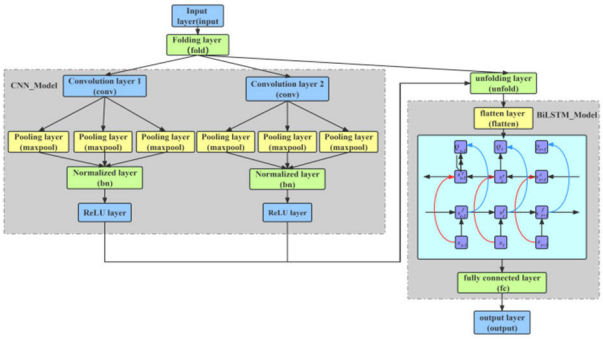


**FIGURE 4.** CNN-BiLSTM model topology.

### D. WHALE OPTIMIZATION ALGORITHM

The initial parameters of the CNN-BiLSTM model such as the number of neurons, InitialLearnRate, L2Regularization, etc., can make a positive impact on the learning of model. For this reason, we use the whale optimization algorithm (WOA) to optimize the initial parameters of the CNN-BiLSTM model for obtaining the optimal parameters. WOA is a new group intelligent optimization algorithm proposed by Mirjalili in 2016. In addition to an easy implementation, the conditions of the objective function are relaxed. The original WOA can provide mathematical models for surrounding prey, spiraling bubbles, and finding prey.

#### 1) ENCIRCLING PREY

In the WOA, the position of each whale represents a feasible solution. Usually during the hunt, whales will randomly choose two behaviors to hunt. In the behavior of whales to

surround prey, whales will randomly choose to drive prey and surround prey towards the optimal position.

The initial position of a general whale is $X_i(x_{i1}, x_{i2}, \ldots, x_{iz})$, which represents each feasible solution, and the optimal position can be found gradually, namely by equations (7) and (8).

$$E = \left|C \cdot X^*(t) - X_i(t)\right| \tag{7}$$

$$X_i(t+1) = X^*(t) - D \cdot E \tag{8}$$

where $E$ represents the distance between the overall optimal position and the individual whale of the population, $X^*(t)$ and $X_i(t)$ are the location of the whale population and individual whale at the $t$ iteration.

$$D = 2a \cdot r - a \tag{9}$$

$$C = 2r \tag{10}$$

For example, in equations (9) and (10), $a$ is the random number uniformly distributed within (0,2). $r$ is the oscillation factor with a random value between 0 and 1.

#### 2) PREDATION MECHANISM

Whales have two feeding mechanisms: a retraction encircling mechanism and a spiral renewal position. From Equation (8), the change of whale position is determined by the convergence factor $E$. When the value of $A$ drops linearly from 2 to 0, whales can achieve the reduction of prey.

As shown in the formula (10), the whale herd in each search for prey, will constantly renew the enclosure, and then constantly spiral upward, until the top of the search is stopped. The reason for adopting the helical updating position mechanism is to simulate the whale feeding process realistically by calculating the optimal distance from individual whales and then establishing a spiral equation for the optimal location of individual whales and populations.

$$X_i(t+1) = E \cdot e^{bl} \cdot \cos(2\pi l) + X^*(t) \tag{11}$$

where $b$ defines the constant of spiral shape; $l$ is a follower of number of machines $[-1, 1]$.

When whales hunting their prey, they will produce bubble nets to attack. They focus on the global optimal location of the population, so the WOA assumes that the ratio of two modes is −1:1. The formula for the calculation of the movement path of the single-headed whale to the global optimal position of the population is expressed as in (12).

$$X_i(t+1) = \begin{cases} X^*(t) - D \cdot Ep < 0.5 \\ E \cdot e^{bl} \cdot \cos(2\pi l) + X^*(t)\, p \geq 0.5 \end{cases} \tag{12}$$

During the hunting phase, in addition to bubble attack, the trigger condition is required at $p < 1$.

#### 3) RANDOM SEARCH

The global random search process equations of WOA are as follows: (13) and (14). The ability of individual whales to randomly update their own positions and moving toward the global optimal position of the population can ensure that the whale population can search for prey in a larger area (with global search capability). Humpback whales need to search for prey through different random ways. As in formula 11, when the convergence factor $|E| < 1$, individual whales will move to the global optimal locations of the population. When the convergence factor $|E| > 1$, individual whales move away from the population, extending the population's search area.

$$E = \left|C \cdot X_{i,rand} - X_i(t)\right| \tag{13}$$

$$X_i(t+1) = x_{i,rand} - D \cdot E \tag{14}$$

where $x_{i,rand}$ is the random position vector of the whale.

## III. QUALITATIVE AND QUANTITATIVE MODELS OF UNCERTAINTY

### A. CLOUD MODEL

The cloud model is a transformation model that represents the uncertainty between a qualitative concept and a quantitative. Let $Q$ be a quantitative domain containing exact numerical values, and $C$ represent the qualitative concept of $Q$. If the quantitative value is $Q = \{x\}$ and $\mu_{\overline{A}}(x) \in [0, 1]$, and the number of $x$ is realized by the first random realization of the concept $C$, then the distribution of $x$ on the quantitative domain $Q$ is called cloud. And, each $x$ is called a cloud droplet.

The application of CM can be measured by three indexes, namely expectation $E_x$, entropy $E_n$, and hyper-entropy $H_e$. $E_x$ is the expectation of the data, as shown in (15). $E_n$ is an index used to measure the ambiguity and probability of qualitative concepts, comprehensively, shown in (16). $E_n$ presents the fuzziness and randomness of data. $H_e$ presents the volatility of data within a certain space, that is, the uncertainty of $E_n$. The magnitude of the value of $H_e$, calculated by (17)-(18), indicates the degree of dispersion and thickness of the cloud. The larger the $H_e$, the greater the cloud thickness, and the greater the degree of dispersion.

$$E_x = \frac{1}{N}\sum_{i=1}^{N} x_i \tag{15}$$

$$E_n = \sqrt{\frac{\pi}{2}} \times \frac{1}{N}\sum_{i=1}^{N} |x_i - E_x| \tag{16}$$

$$S^2 = \frac{1}{N-1}\sum_{i=1}^{N} (x_i - E_x)^2 \tag{17}$$

$$H_e = \sqrt{S^2 - E_n^2} \tag{18}$$

where $e_{up}$ is the $i^{th}$ sample value, $e_{up}$ is the sample volume, and $e_{up}$ is the sample variance.

For $H_e$, it is imaginary when $S^2 - E^2 < 0$. To solve this issue, another computation is proposed to ensure $H_e$ be real always.

$$H_e = \sqrt{\left|S^2 - E_n^2\right|} \tag{19}$$

Generally, cloud models are separated to forward CM and reverse CM, both of which can realize qualitative and quantitative conversion. The forward CM is comprised of the formulas (20)-(22). Based on forward cloud and reverse cloud, the Gaussian cloud is adopted in this study to analyze the WFPF uncertainty. Fig. 5 shows the Gaussian cloud, and its expectation curve follows a Gaussian distribution. It can clearly reflect the quality of the WFPF results and how the uncertainty fluctuates. And, this study adopted the Gaussian cloud to analyze the uncertainty of error distribution qualitatively.

$$E_{nn} = rand\ (1) \times H_e + E_n \tag{20}$$

$$x = rand\ (1) \times E_{nn} + E_x \tag{21}$$

$$y = e^{\frac{-(x-Ex)\wedge 2}{2Enn\wedge 2}} \tag{22}$$

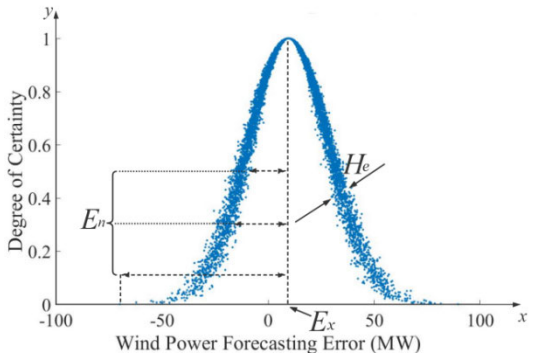


**FIGURE 5.** Cloud model schematic.

### B. NON-PARAMETRIC KERNEL DENSITY ESTIMATION

Regarding the difficulty in quantifying the uncertainty of WFPF, the uncertainty of WFPF can be further quantified by NPKDE and confidence interval.

NPKDE is attractive because it does not require assumptions to be made about the distribution. It only requires the selection of a kernel function, where each kernel function produces a different distribution. Thus, the kernel function chosen for this study is the following Gaussian kernel function:

$$g\left(x\right) = \frac{1}{\sqrt{2\pi}\sigma}\exp\left(-\frac{(x-\mu)^2}{2\sigma^2}\right) \tag{23}$$

where $\mu$ represents the mean value of WFPF error, and $\sigma$ is the standard deviation. The probability density distribution function of NPKDE is

$$f(x) = \frac{1}{N}\sum_{i=1}^{N} \mathrm{g}\left(\frac{x-x_i}{h}\right) \tag{24}$$

where $N$ is the number of interval samples, and $h$ is the bandwidth coefficient.

After the probability distribution is obtained, the confidence interval is used to calculate it quantitatively.

The WFPF error is defined as the difference between the WFPF value $P_{\text{fore}}$ and the wind power real value $P_{\text{ture}}$ at a certain time point, i.e., $e = P_{\text{fore}} - P_{\text{true}}$. The confidence level for the wind power error is calculated as follows:

$$P\left(e_{\text{low}} < e < e_{\text{up}}\right) = 1 - \theta \tag{25}$$

In Eq.(25), the confidence interval $[e_{\text{low}}, e_{\text{up}}]$ is given with the confidence level $1-\theta$. $P\left(e_{\text{low}} < e < e_{\text{up}}\right)$ means the probability of WFPF error $e$ falling within the interval $[e_{\text{low}}, e_{\text{up}}]$. And, the confidence interval for WFPF is $[P_{\text{fore}} - e_{\text{low}}, P_{\text{fore}} - e_{\text{up}}]$.

For the modeling of uncertainty analysis, the holistic error modeling cannot satisfy the demonstration of high reliability and adaptability at all model. To tackle this issue, hybrid modeling with CM and NPKDE is proposed for qualitative-to-quantitative analysis, particularly in short-term WFPF uncertainty analysis. This new analysis approach can make the forecasting more comprehensive and distinct.

## IV. DATA ANALYSIS AND PARAMETER SETTINGS

### A. DATA SETS AND PARAMETER SETTINGS

This study utilizes wind power data from a wind farm in northern China, located in [114°E, 41°N]. The wind farm covers an area of about 100 square kilometers and has 90 wind turbines. The diameter and height of the wind turbine are 70.5 m and 67 m, respectively, and the output power of a single wind turbine is 1.5 MW.

The WFPF data with a time resolution of 15 minutes includes wind farm unit operation data, unit attributes and NWP data. The data comes from the wind farm's monitoring and data acquisition system. It is obtained from the data center (http://www.cma.gov.cn) with 1 km spatial resolution. As wind power is affected by wind speed and direction, the WFPF based on NWP data has been proven to be reasonable and feasible. It is the means of the NWP data from these spatial grid points with the attributes including barometric pressure, wind speed, temperature and wind direction.

The WFPF data span the period from January 1, 2010, to August 31, 2011, which are divided into a training set and a test set. The training set consists of NWP data for the whole year of 2010 and wind power data for one year. After data processing, 25384 groups of data were retained for experiment. The test lasted for 243 days from January 1 to August 31, 2011. In this study, 4-hour, 24-hour and 72-hour forecast data samples were selected for winter (Feb. 13-15th, 2011) and summer (Jun.17-19th, 2011) to verify the validity and performance of the model on multiple time scales and seasons.

### B. EVALUATION METRICS

Figs. 6(a) and (b) show the wind speed on February 13-15 and June 17-19 respectively. Since the wind speeds and the NWP are highly correlated, the trend and magnitude of fluctuations in NWP wind speed and wind mast show almost identical. The variation of the NWP data appears smoother than that of the wind gauge mast data. Meanwhile, both wind speed and

wind direction impact the wind power generation and thus the utilization of wind speed and wind direction in NWP for WFPF is reasonable and feasible.

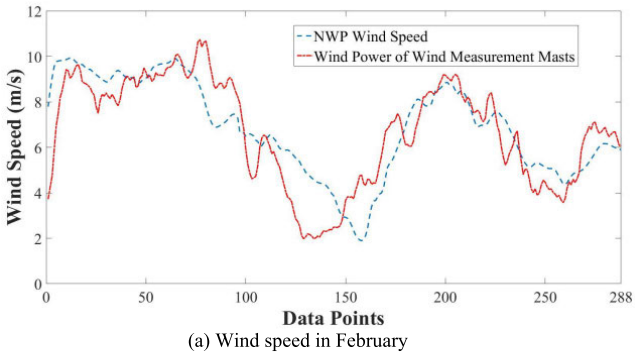


(a) Wind speed in February

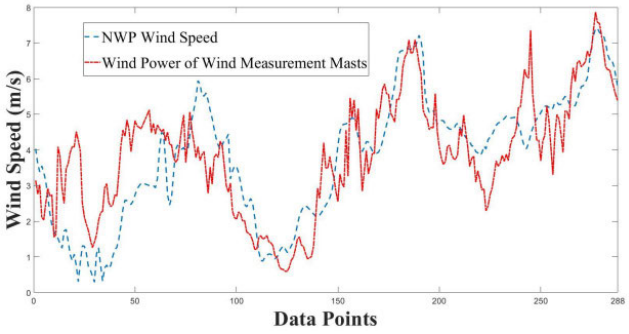


(b) Wind speed in June

**FIGURE 6.** NWP wind speed versus wind speed at the wind measurement mast.

## V. RESULTS AND COMPARISONS

### A. SHORT-TERM WFPF ANALYSIS

#### 1) INTERNAL STRUCTURAL ANALYSIS OF THE CNN-BILSTM

To verify the improvement of CNN-BiLSTM in WFPF accuracy, this study compares the proposed CNN-BiLSTM model containing an MCP structure, to the CNN-BiLSTM models with three other internal structures: single-convolution (SC), single-convolution and single-pooling (SCP), and single-convolution and multi-pooling (SCMP). As shown in TABLE 2, $ mean$ is the mean value of RMSE; *SD* is the standard deviation of RMSE; 25%, 50%, and 75% are the confidence levels of RMSE; *min* and *max* are the minimum and maximum values of RMSE. These parameters provide a comprehensive description for the distribution of the RMSE of WFPF. Five characteristic values (minimum, upper quartile, median, lower quartile, and maximum) are used to describe the forecasting effects of wind power in different situations. Box plots are used to identify data symmetry, data dispersion, skewness, and tail weight.

As shown in TABLE 2, with the increase of convolution kernel and pooling operation, the RMSE mean value and standard deviation of the model become smaller, where the MCP value is minimum and interval stable. Since the CNN-BiLSTM with MCP is able to extract more feature parameters, it can better map the relationship with the output values in learning process.

**TABLE 2.** Results of CNN-BiLSTM models with four internal structures.

| | SC | SCP | SCMP | MCP |
|---|---|---|---|---|
| Count | 5 | 5 | 5 | 5 |
| Mean (%) | 10.9888 | 10.5414 | 10.2644 | 9.8783 |
| SD (%) | 2.0306 | 1.9514 | 0.9786 | 0.4066 |
| Min (%) | 10.77 | 10.1686 | 9.7089 | 9.385 |
| 25% | 10.7994 | 10.3333 | 10.0377 | 9.7055 |
| 50% | 10.8646 | 10.6576 | 10.3815 | 9.8457 |
| 75% | 11.0789 | 10.7164 | 10.5176 | 10.020 |
| Max (%) | 11.5925 | 10.8061 | 10.5914 | 10.4822 |

The box plot in Fig. 7 indicates the RMSE fluctuations of the CNN-BiLSTM with different convolution and pooling layers. It can be seen that MCP box is the shortest and RMSE average is the lowest.The CNN-BiLSTM with MCP also shows a higher stability of forecasting than that of the CNN-BiLSTM with SCP, which is consistent with the description in TABLE 2.

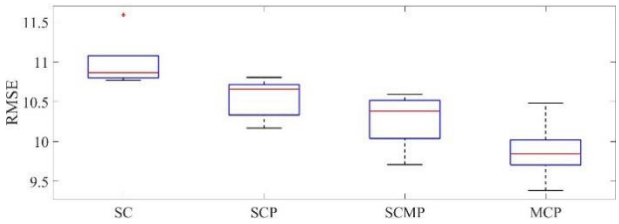


**FIGURE 7.** NWP CNN-BiLSTM box diagram of forecasting results under different internal structures.

**TABLE 3.** The RMSE and MAE values of 4-hour WFPF model.

| Month | Time Span | Model | RMSE | MAE |
|---|---|---|---|---|
| Feb | 4 hours | CNN-BiLSTM | 4.1312 | 3.5571 |
| | | WOA-CNN-BiLSTM | 3.1757 | 3.4240 |
| | | BELM | 5.5711 | 5.0753 |
| | | LSTM | 6.2733 | 5.8576 |
| | | PSO-BP | 8.6490 | 8.2836 |
| | | BP | 9.7682 | 9.4402 |
| | | WNN | 9.4846 | 8.0052 |
| Jun | 4 hours | CNN-BiLSTM | 3.7936 | 3.4652 |
| | | WOA-CNN-BiLSTM | 3.7731 | 3.3313 |
| | | CNN-LSTM | 3.8822 | 3.6173 |
| | | BiLSTM | 4.0732 | 3.8075 |
| | | LSTM | 4.1321 | 3.7035 |
| | | BELM | 3.8020 | 3.3615 |
| | | PSO-BP | 4.8542 | 4.5329 |
| | | BP | 4.6736 | 4.1562 |
| | | WNN | 8.4610 | 7.4102 |

#### 2) ANALYSIS OF SHORT-TERM WFPF

Fig. 8(a) and (b) show the 4-hour WFPF results on February 13 and June 18, respectively. The red dashed line is the WOA-CNN-BiLSTM; the red solid line is the CNN-BiLSTM model; the yellow solid line is the BELM model; the purple line is the WNN model; and the green line is the BP

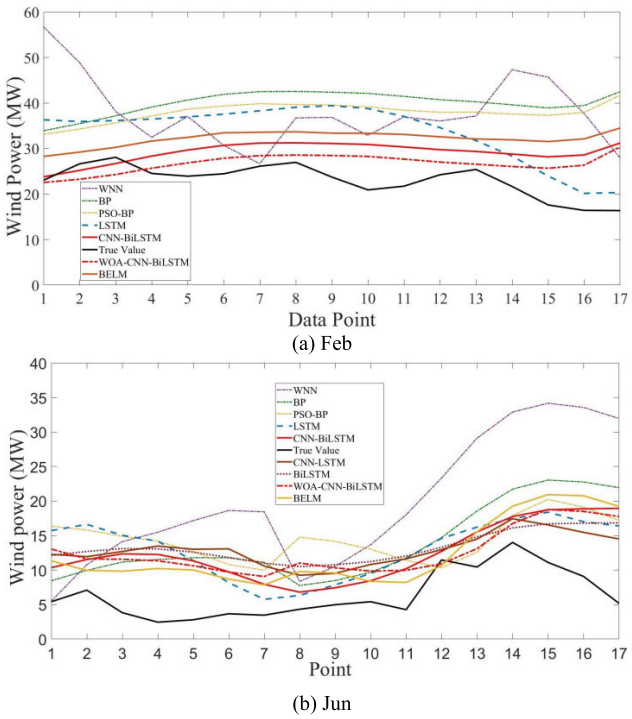


(a) Feb

(b) Jun

**FIGURE 8.** 4-hour WFPF results.

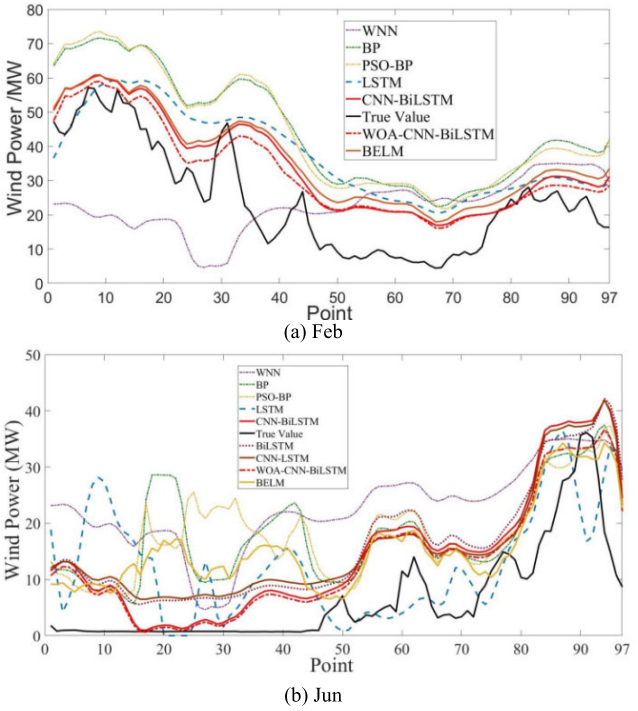


(a) Feb

(b) Jun

**FIGURE 9.** 24-hour WFPF results.

**TABLE 4.** The RMSE and MAE values of 24-hour WFPF results.

| Month | Time Span | Model | RMSE | MAE |
|---|---|---|---|---|
| Feb | 24 hours | CNN-BiLSTM | 6.8078 | 5.8064 |
| | | WOA-CNN-BiLSTM | 5.9545 | 4.9316 |
| | | BELM | 7.6062 | 6.6471 |
| | | LSTM | 8.8697 | 7.5984 |
| | | PSO-BP | 11.9546 | 11.1665 |
| | | BP | 12.1013 | 11.3781 |
| | | WNN | 16.6055 | 15.7701 |
| Jun | 24 hours | CNN-BiLSTM | 5.3477 | 4.3777 |
| | | WOA-CNN-BiLSTM | 4.5287 | 3.7011 |
| | | CNN-LSTM | 5.5457 | 5.5457 |
| | | BiLSTM | 5.8867 | 5.8867 |
| | | LSTM | 6.09 | 4.8690 |
| | | BELM | 5.8063 | 5.2553 |
| | | PSO-BP | 7.4952 | 6.6309 |
| | | BP | 7.5026 | 6.4130 |
| | | WNN | 9.5037 | 8.8659 |

model, etc. TABLE 3 compares the RMSE and MAE for 4-hour WFPF models. The WOA-CNN-BILSTM has better performance than other six models, with the minimum of RMSE and MAE, followed by the CNN-BILSTM model. Meanwhile, it can be seen from Figure 12 that the trend of the red line is most similar to the real value. Although there are some errors between the forecasted results and the real values. Because the wind speed can be influenced by the topography and the wake in wind farm, and characterized by some randomness that can cause forecasting and measuring errors.

Figs. 9(a) and (b) show the 24-hour WFPF results on February 13 and June 18. The RMSE and MAE values of the five models in the 24-hour forecasting are listed in TABLE 4. In these cases, the WOA-CNN-BiLSTM model also achieves the highest forecasting accuracy in the 24-hour WFPF.But the 24-hour forecast has a significantly larger effect and range of fluctuations than the 4-hour forecast, with a noticeable improvement in RMSE and MAE values.

Figs. 10(a)-(b) and TABLE 5 display the 72-hour WFPF covering the two periods of February 13-15 and of June 17-19, respectively. It can be seen that the forecast power curve is smoother than the actual power curve. This is because NWP data is processed as forecast data and is smoother than the actual wind speed in Fig. 6(a) and 8(b). The fluctuation and variation trend of the predicted curve are basically consistent with the actual curve. This proves the correctness of WFPF model. Although the RMSE and MAE forecasting errors for 72 hours continue to be significantly high, the degree of increase in RMSE and MAE is noticeably lower compared to 4 hours and 24 hours.

However, it should be noted that the forecasting power of WOA-CNN-BiLSTM in Fig. 10(b) from the 100th data point to the 150th data point is consistent with the NWP fluctuations, unlike the other four forecasting models. This is because of the advantages of CNN-BiLSTM in feature selection and learning. Specifically, WOA-CNN-BiLSTM can use not only the learning capability of BiLSTM but also the features extracted by the CNN for further learning to remove the uncertainty from the forecasting and achieve more consistency with the forecasting pattern. Between the 150th and 200th data points shown in Fig. 10(a), this capability is proved again.

From Figs. 8-10 and TABLE 2-4, the errors of WOA-CNN-BiLSTM model are smaller than those of the other four models at different time scales, which indicates that WOA-CNN-BiLSTM can obtain higher forecasting accuracy in short-term WFPF than other four models. At the same time, it was discovered through research that as the forecasting time scale increases, the WFPF's predicted RMSE and MAE values significantly increase. However, the rate of improvement shows a negative correlation trend. Moreover, the predicted RMSE and MAE values for WOA-CNN-BiLSTM remain stable within 9%.

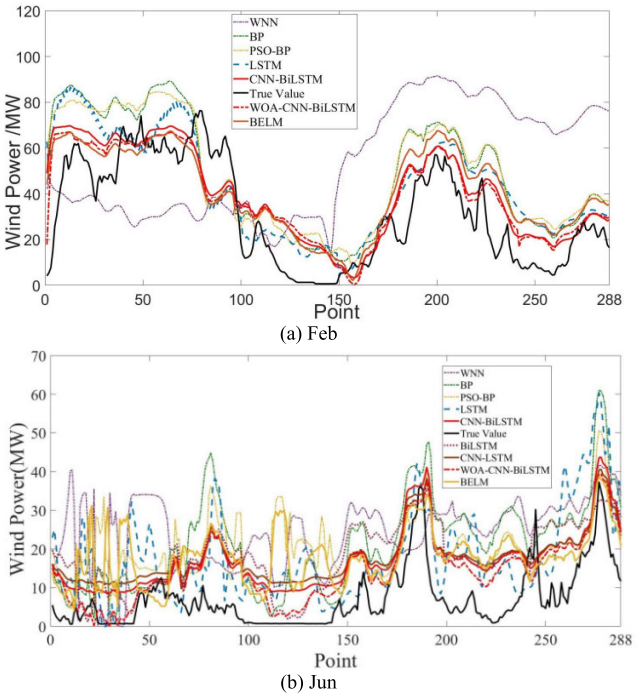


**FIGURE 10.** 72-hour WFPF results.

**TABLE 5.** The RMSE and MAE values of 72-hour WFPF results.

| Month | Time Span | Model | RMSE | MAE |
|---|---|---|---|---|
| Feb | 72 hours | CNN-BiLSTM | 8.5387 | 6.9268 |
| | | WOA-CNN-BiLSTM | 8.0458 | 6.5738 |
| | | BELM | 9.431 | 8.0218 |
| | | LSTM | 10.1868 | 7.8631 |
| | | PSO-BP | 12.4727 | 11.0033 |
| | | BP | 12.6319 | 8.4166 |
| | | WNN | 23.2602 | 20.8538 |
| Jun | 72 hours | CNN-BiLSTM | 6.0197 | 5.5160 |
| | | WOA-CNN-BiLSTM | 5.1260 | 4.3767 |
| | | CNN-LSTM | 6.3689 | 6.3689 |
| | | BiLSTM | 7.0614 | 6.1890 |
| | | LSTM | 7.6317 | 6.2173 |
| | | BELM | 7.2338 | 6.2699 |
| | | PSO-BP | 7.4952 | 7.2451 |
| | | BP | 8.2313 | 7.6993 |
| | | WNN | 10.7492 | 9.7047 |

We found from TABLE 6 that the maximum error peak of WOA-CNN-BiLSTM is the smallest at different time scales. In addition, various indicators such as expectation, entropy, super-entropy, RMSE, and MAD are used to mutually corroborate and further demonstrate the quality and performance of this model.

**TABLE 6.** Maximum peak error at different time scales.

| | | Model | 4 hours | 24 hours | 72 hours |
|---|---|---|---|---|---|
| Maximum error peak | Feb | WOA-CNN-BiLSTM | 14.01 | 27.37 | 27.37 |
| | | CNN-BiLSTM | 14.84 | 29.16 | 31.29 |
| | | LSTM | 17.87 | 34.79 | 58.72 |
| | | PSO-BP | 25.36 | 43.77 | 64.02 |
| | | BP | 26.13 | 44.69 | 63.60 |
| | | WNN | 33.67 | 44.58 | 68.94 |
| | | BELM | 18.13 | 32.56 | 32.56 |
| | Jun | WOA-CNN-BiLSTM | 10.58 | 21.13 | 20.03 |
| | | CNN-BiLSTM | 13.768 | 23.42 | 20.12 |
| | | CNN-LSTM | 11.03 | 24.92 | 21.48 |
| | | BiLSTM | 11.66 | 26.83 | 23.11 |
| | | LSTM | 11.22 | 27.42 | 34.45 |
| | | PSO-BP | 12.01 | 23.65 | 33.44 |
| | | BP | 16.76 | 27.88 | 32.91 |
| | | WNN | 26.78 | 22.43 | 32.16 |
| | | BELM | 14.05 | 22.00 | 30.09 |

To further verify the variability of the forecasting across the individual models. The author employed a T-test to assess the significance of differences in forecasting errors and RMSE results for June data from the same sample. A p-value $p \leq 0.05$ led to the rejection of the null hypothesis, indicating a significant difference in the predictive outcomes of the two models. Conversely, a p-value $p \geq 0.05$, resulted in the acceptance of the null hypothesis, suggesting no significant difference between the models' forecastings. As presented in TABLE 7 there were statistically significant differences between the WOA-CNN-BiLSTM model and other models in terms of 72-hour and 24-hour forecasts for both forecasting error and RMSE, with negative t-values, indicating that the mean forecasting error and RMSE of the WOA-CNN-BiLSTM model were lower than those of the other models, thus confirming its superior predictive performance.

Furthermore, at the 4-hour forecast interval, comparisons with all models except the WNN model yielded p-values $p \geq 0.05$, with negative t-values. Considering that the forecasting error was measured in MW, and the base values could be small, the lack of significance could be attributed to an insufficient sample size. To further substantiate the predictive differences at the 4-hour mark, we recalculated the T-test after converting the forecasting error unit to KW. As shown in

**TABLE 7.** MW level T-test distribution.

| Time | Model | Error | | RMSE | |
|---|---|---|---|---|---|
| | | p | t | p | t |
| 72 hours | CNN-BiLSTM | 1.13E-07 | -5.3724 | 0.006 | -3.3297 |
| | CNN-LSTM | 3.06E-14 | -7.7941 | 0.0027 | -3.7573 |
| | BiLSTM | 3.62E-12 | -7.1034 | 0.0005 | -4.7425 |
| | LSTM | 8.62E-09 | -5.8426 | 0.0001 | -5.5894 |
| | BELM | 2.70E-12 | -7.1474 | 0.0008 | -4.4150 |
| | PSO-BP | 7.84E-23 | -10.2707 | 0.0002 | -5.4136 |
| | BP | 3.78E-23 | -10.3539 | 4.30E-05 | -6.243 |
| | WNN | 7.77E-42 | -16.9121 | 3.63E-04 | -4.9051 |
| 24 hours | CNN-BiLSTM | 0.0101 | -2.6464 | 0.0217 | -2.6361 |
| | CNN-LSTM | 3.86E-04 | -3.6132 | 0.019 | -2.7091 |
| | BiLSTM | 1.07E-04 | -3.9574 | 0.0118 | -2.9674 |
| | LSTM | 0.0396 | -2.0721 | 0.007 | -3.2432 |
| | BELM | 3.49E-05 | -4.2389 | 0.0057 | -3.3621 |
| | PSO-BP | 4.32E-10 | -6.582 | 3.77E-03 | -3.5819 |
| | BP | 1.87E-08 | -5.871 | 4.25E-03 | -3.516 |
| | WNN | 6.11E-27 | -12.6063 | 1.93E-04 | -5.2862 |
| 4 hours | CNN-BiLSTM | 0.8212 | -0.2279 | 0.0421 | -2.275 |
| | CNN-LSTM | 0.6597 | -0.4445 | 0.0248 | -2.5634 |
| | BiLSTM | 0.4112 | -0.8327 | 0.0085 | -3.1406 |
| | LSTM | 0.5633 | -0.584 | 0.0018 | -3.9911 |
| | BELM | 0.962 | -0.048 | 3.92E-04 | -4.8593 |
| | PSO-BP | 0.0616 | -1.9373 | 2.74E-04 | -5.0722 |
| | BP | 0.2434 | -1.1884 | 1.61E-04 | -5.398 |
| | WNN | 8.88E-04 | -3.6652 | 4.27E-06 | -7.9008 |

TABLE 8, at the KW level, the WOA-CNN-BiLSTM model exhibited significant differences compared to other models, with p-values $p \leq 0.05$ and negative t-values, affirming that the WOA-CNN-BiLSTM model had lower mean forecasting errors and RMSE for the 4-hour forecasts as well.

To further demonstrate the optimal effect of WOA, we selected PSO, Grey Wolf Optimizer (GWO) and non-optimized algorithms for result comparisons. As can be seen from Figure 11 and TABLE 9, the forecasting results with the optimized model are shown better than those of the non-optimized model. Particularly, the WOA group intelligent

**TABLE 8.** KW level T-test distribution.

| Time | Model | Error | |
|---|---|---|---|
| | | p | t |
| 4 hours | CNN-BiLSTM | 3.32E-09 | -8.062 |
| | CNN-LSTM | 2.80E-10 | -8.9994 |
| | BiLSTM | 7.19E-11 | -9.5341 |
| | LSTM | 2.52E-08 | -7.3224 |
| | BELM | 1.14E-07 | -6.7849 |
| | PSO-BP | 5.76E-11 | -9.6229 |
| | BP | 4.32E-08 | -7.1297 |
| | WNN | 7.67E-08 | -6.9255 |

optimization algorithm is tested with the best effects, prior to the GWO optimization algorithm and the PSO algorithm.

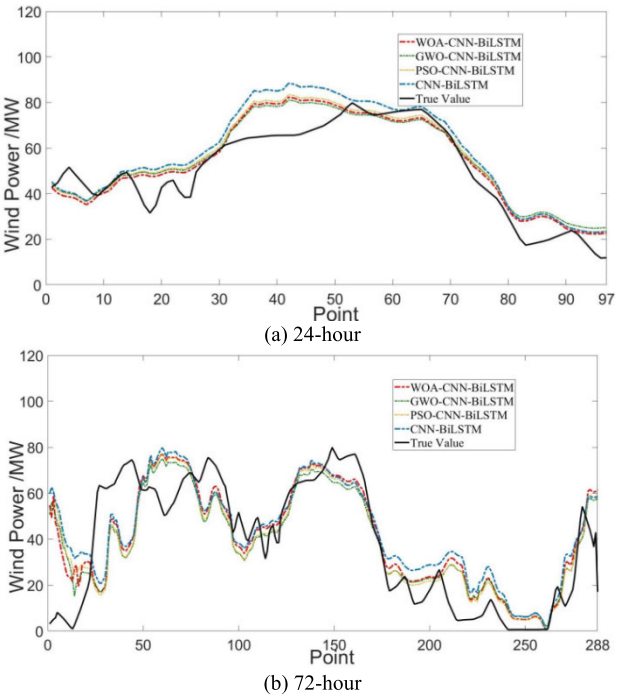


(a) 24-hour

(b) 72-hour

**FIGURE 11.** Comparison of CNN-BiLSTM model under different optimization algorithms.

**TABLE 9.** The RMSE and MAE values of 72-hour WFPF results.

| Month | Time Span | Model | RMSE | MAE |
|---|---|---|---|---|
| May | 24 hours | WOA-CNN-BiLSTM | 4.3995 | 3.4916 |
| | | GWO-CNN-BiLSTM | 4.5246 | 3.7156 |
| | | PSO-CNN-BiLSTM | 4.7670 | 3.7775 |
| | | CNN-BiLSTM | 5.7974 | 4.6154 |
| May | 72 hours | WOA-CNN-BiLSTM | 8.7190 | 6.472 |
| | | GWO-CNN-BiLSTM | 8.9616 | 6.6588 |
| | | PSO-CNN-BiLSTM | 9.2561 | 6.6845 |
| | | CNN-BiLSTM | 9.6917 | 7.4589 |

To improve the practicality of the validation forecasting algorithm, we compared it with the most advanced technologies, namely Generative Adversarial Networks (GAN) and

**TABLE 10.** The RMSE and MAE values of 72-hour WFPF results.

| | Time | GAN | GNN | CNN-BiLSTM |
|---|---|---|---|---|
| RMSE | 1.26 | 7.3193 | 7.0609 | 6.8861 |
| | 2.01 | 9.4329 | 9.9463 | 9.6631 |
| | 3.04 | 10.9231 | 10.6844 | 10.092 |
| | 4.01 | 6.1026 | 5.8108 | 5.7291 |
| | 6.02 | 6.8879 | 6.7876 | 7.0236 |

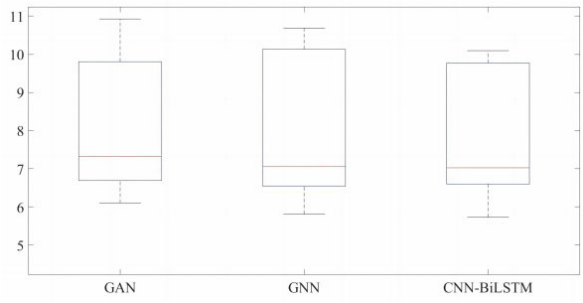


**FIGURE 12.** The box diagram of RMSE effect predicted by CNN-BILSTM and LSTM models under different forecast data conditions.

**TABLE 11.** Comparison of RMSE results between CNN-BILSTM and GAN and GNN with different data conditions.

| | GAN | GNN | CNN-BILSTM |
|---|---|---|---|
| Count | 5 | 5 | 5 |
| Mean (%) | 8.1332 | 8.1332 | 8.0580 |
| std (%) | 1.8987 | 1.9880 | 2.1285 |
| Min (%) | 5.7291 | 6.1026 | 5.8108 |
| 25% | 6.5969 | 6.6916 | 6.5434 |
| 50% | 7.0236 | 7.3193 | 7.0609 |
| 75% | 9.7703 | 9.8055 | 10.1308 |
| Max (%) | 10.0920 | 10.9231 | 10.6844 |
| loss | 2000 | 2500 | 2800 |

Graph Neural Networks (GNN). We found that the CNN-BiLSTM model performs the best in overall forecasting capability for WFPF.

The reason why CNN-BiLSTM is chosen as the forecasting model is that in terms of forecasting strategy, in the field of wind power forecasting, the stability of the hybrid model for wind farm power forecasting is higher than that of a single model, as shown in TABLE 10, TABLE 11 and Figure 12. Random selection After five days of data for forecasting, GAN, GNN, and CNN-BiLSTM have their advantages and disadvantages in forecasting accuracy in multiple forecastings, but CNN-BiLSTM is slightly better than these two algorithms in terms of forecasting stability. The reason is that the actual wind farm data has strong uncertainty due to the influence of terrain wind speed, and this problem is difficult to eliminate its influence in the learning of a single model.

In addition, LSTM, BILSTM CNN-LSTM algorithm, as a classic algorithm of deep learning, has been used in recent years, which can reflect the advantages of the current use of the algorithm. For example, we have investigated and done some related projects to show: the UK wind farm forecasting system some uses the Xgboost algorithm. The forecasting systems used by the subordinate wind power in China include IPSO-LSTM-GMM, IPSO-GRU forecasting system, etc., which are more suitable algorithms for local application after testing, and have higher priorities.

Here, all test cases take the short-term forecast of large wind farm as a classic example. Regarding to the current wind farm operation, it requires the coming three-day forecasting to ensure the power supply quality. The real wind power data from wind farms are different from the simulation data, generally affected by the influence of power supply and demand and even the fan damage. Besides, all power generation units in a wind farm are not run fully in 24 hours, which leads to the power outputs unstable and produce large fluctuations on other time scales (e.g. 24-hour, 72-hour). After multiple test analysis, it is found that the WOA-CNN-BILSTM model remains some deviations in actual forecasting. Thus, the WFPF uncertainty analysis is performed for the characteristic determination of WFPF results.

### B. UNCERTAINTY ANALYSIS FOR WFPF

#### 1) UNCERTAINTY ANALYSIS BASED ON CLOUD MODEL

To further analyze the uncertainty of WFPF, we propose using the CM method to describe WFPF errors. Figs. 13 show the cloud droplet diagrams of the forecasting models for comparisons, including LSTM, BP, PSO-BP, WNN, and CNN-BiLSTM and WOA-CNN-BiLSTM and BELM. The forecasting time span is set to 4 hours.

As Fig. 8 cannot directly reflect the randomness and volatility of each model, the data analysis displays the cloud droplet diagrams in Fig. 13 to show the error distribution of WOA-CNN-BiLSTM clearly. And, the forecasting errors from GAN, GNN and CNN-BILSTM in TABLE 7 are used to evaluate the quality of the models.

The minimum entropy and super-entropy values of WOA-CNN-BiLSTM represent the minimum randomness and volatility of the model forecasting, which shows the superiority of WOA-CNN-BiLSTM.

Figs. 14-15 show the cloud droplets of 24-hour and 72-hour forecasting errors. It can be seen that the expectation, entropy, and super-entropy of WOA-CNN-BiLSTM's forecasting error display smaller than those of other models at different time scales. It is further proved that the performance of WOA-CNN-BiLSTM is superior to other models.

The characteristics of the CM values of the forecasting errors of the five models at different time scales are shown in TABLE 12. The eigenvalues of the CM values of WFPF errors for WOA-CNN-BiLSTM are smaller than those of the other four models for the three forecasting time scales in February and June.

Particularly, the distribution law of CM's digital characteristics is determined from the WFPF results of all models as follows:

1) When the forecasted power value is greater than the actual wind power output, the expectation of CM should be

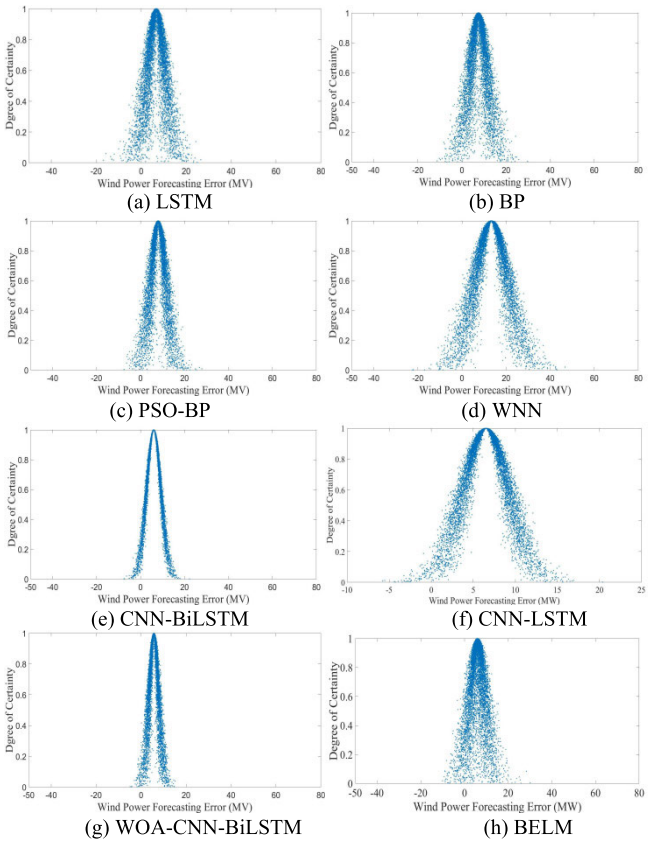


**FIGURE 13.** The cloud droplets of 4-hour WFPF errors in June.

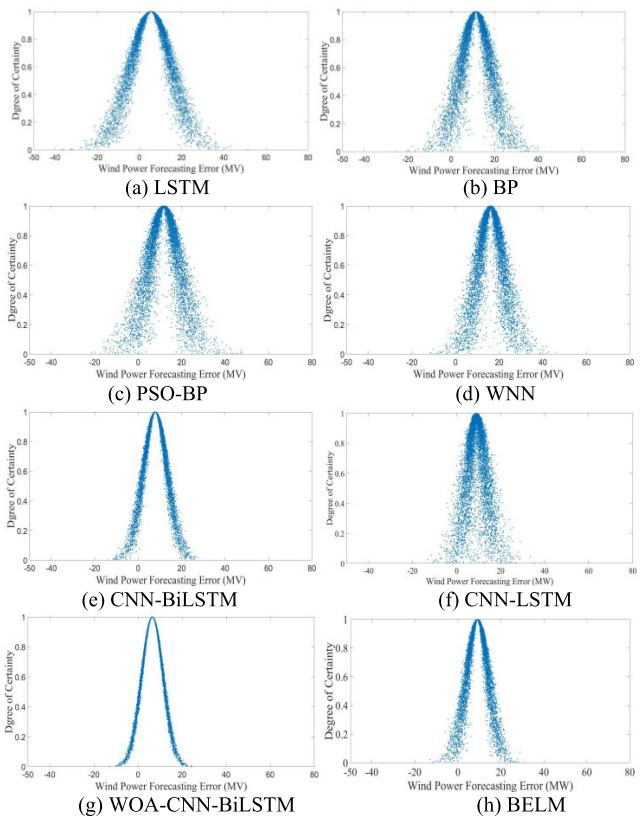


**FIGURE 14.** The cloud droplets of 24-hour WFPF error in June.

a positive value. The absolute value of the expected value become smaller, which can lead to a smaller mean error.

2) The entropy value reflects the concentration of the probability density distribution of the WFPF. The entropy value tends to be larger, which makes the shape of the distribution curve become sharper. When the distribution gets sharper, the confidence interval shrinks.

3) The super entropy tends to be smaller, which indicates the cohesiveness of the distribution curve is improved. There exists the situation that the forecasting errors between the real output and the forecasting values become minor, and the volatility of these errors lessens.

This part of analysis has proved that the CM can provide more directional evaluation characteristics than the classic model evaluation measure in WFPF, namely, the average value of error amplitude, the amplitude fluctuation range, and the randomness of the amplitude fluctuation. The WFPF cloud theory, i.e., the forecasting distribution and characteristics, can be further used to perform the probability joint distribution forecasting and the coupling characteristics analysis.

### 2) CONFIDENCE INTERVAL OF WFPF

As the probability density distribution of WFPF errors would be determined through the NPKDE method, the confidence intervals are computed here for the further discussions of the uncertainty analysis. Figs. 16(a) and (b) show the probability density distributions of 24-hour and 72-hour WFPF errors,

**TABLE 12.** The characteristics of CM with four models in June.

| Time | Model | Ex | En | He |
|---|---|---|---|---|
| 4 hours | CNN-BiLSTM | 5.99 | 3.26 | 0.37 |
| | WOA-CNN-BiLSTM | 6.17 | 2.51 | 0.28 |
| | CNN-LSTM | 6.51 | 2.67 | 0.53 |
| | BiLSTM | 6.85 | 2.61 | 0.63 |
| | LSTM | 6.67 | 3.72 | 1.51 |
| | PSO-BP | 8.03 | 3.37 | 1.16 |
| | BELM | 5.96 | 3.07 | 1.63 |
| | BP | 7.48 | 3.56 | 3.64 |
| | WNN | 13.34 | 7.36 | 1.81 |
| Jun, 4 hours | CNN-BiLSTM | 7.87 | 4.5 | 0.7 |
| | WOA-CNN-BiLSTM | 6.52 | 4.42 | 0.26 |
| | CNN-LSTM | 9.01 | 4.9 | 1.16 |
| | BiLSTM | 9.4 | 4.76 | 1.2 |
| | LSTM | 9.68 | 5.45 | 1.6 |
| | PSO-BP | 11.77 | 6.95 | 2.08 |
| | BELM | 9.11 | 5.05 | 0.98 |
| | BP | 11.38 | 6.72 | 1.79 |
| | WNN | 16.08 | 5.59 | 1.77 |
| 72 hours | CNN-BiLSTM | 9.74 | 4.46 | 1.6 |
| | WOA-CNN-BiLSTM | 7.36 | 4.07 | 1.41 |
| | CNN-LSTM | 10.57 | 5.45 | 1.78 |
| | BiLSTM | 10.8 | 6.99 | 1.96 |
| | LSTM | 10.35 | 8.88 | 1.77 |
| | PSO-BP | 12.74 | 7.24 | 2.26 |
| | BELM | 10.65 | 7.71 | 2.45 |
| | BP | 13.71 | 9.13 | 2.54 |
| | WNN | 16.89 | 9.81 | 2.60 |

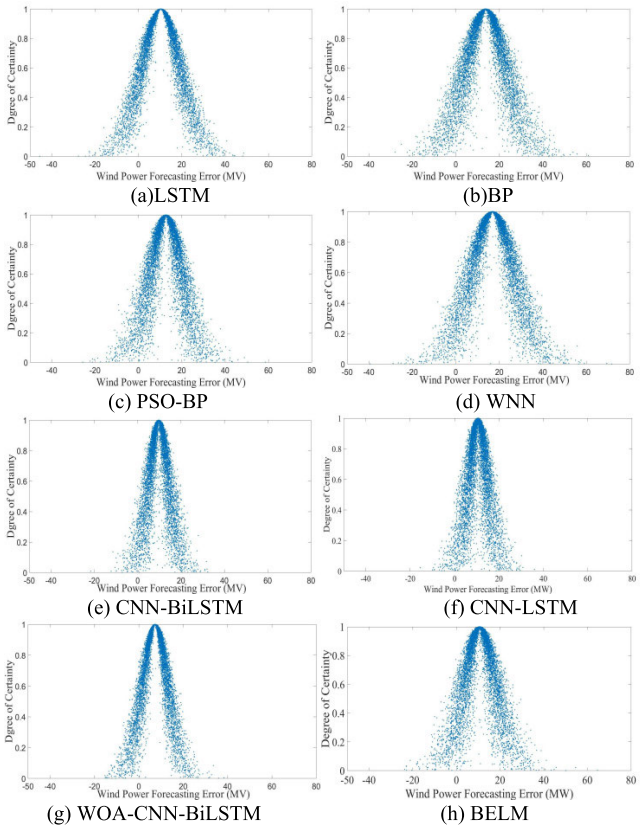


**FIGURE 15.** The cloud droplets of 72-hour WFPF error in June.

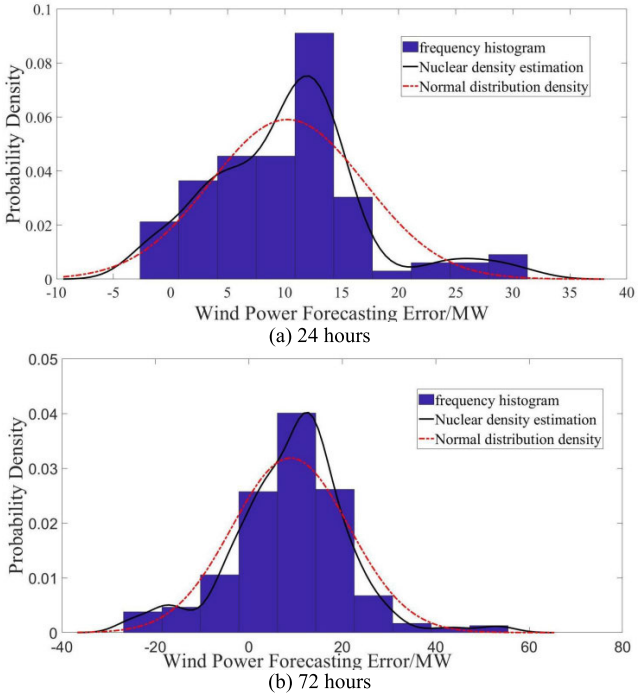


**FIGURE 16.** Probability density distribution of WFPF errors.

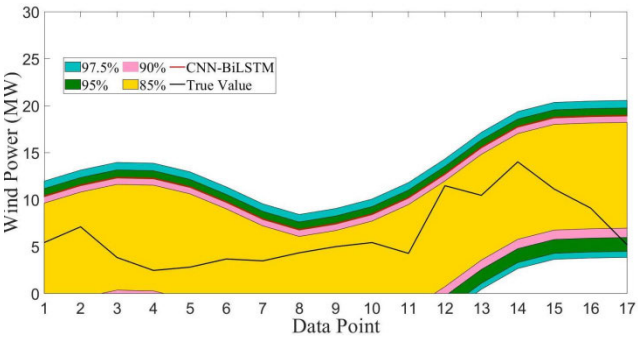


**FIGURE 17.** Confidence levels for 4-hour WFPF by CNN-BiLSTM.

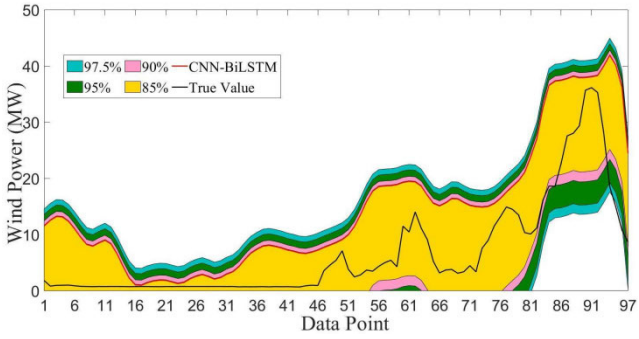


**FIGURE 18.** Confidence levels for 24-hour WFPF by CNN-BiLSTM.

respectively. All plots show that the probability density distribution can characterize the distribution of WFPF errors accurately.

The confidence intervals of 4-hour, 24-hour, and 72-hour WFPF results can be obtained by NPKDE. Figs.17-19 show the confidence interval distributions of CNN-BiLSTM at 97.5%, 95%, 90%, and 85% confidence levels, respectively.

It can be seen that the confidence interval reliability of the 4-hour WFPF is higher than that of the 24-hour and 72-hour WFPF. This is because with the increase of time span, the fluctuation degree on the forecasting values and the real values becomes larger, which increases the forecasting difficulty. This further confirms the qualitative analysis of WFPF by cloud model. The quantitative analysis results of NPKDE show higher interval accuracy at different time scales, making the probability of WFPF falling into the confidence interval greater than the current confidence level. However, there exists some of WFPF excluded in the confidence interval due to sudden changes in actual output power, e.g. NWP errors, the changes of unit operating conditions, and wind gusts. In addition, the increases of confidence level can enlarge the width of the confidence interval, which can increase the reliability of the WFPF values.

Table 13 lists the coverage rates of confidence intervals for WFPF based on CNN-BiLSTM at 4-hour, 24-hour, and 72-hour time scales. The coverage rate $\partial_P$ is consistently higher than the confidence level, which verifies that the confidence interval method based on NPKDE can accurately describe the distribution range of the actual output power of the wind farm.

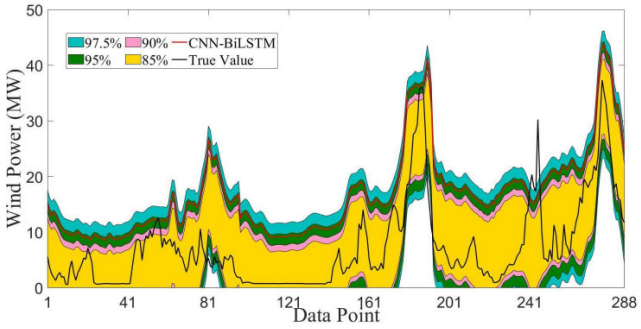


**FIGURE 19.** Confidence levels for 24-hour WFPF by CNN-BiLSTM.

**TABLE 13.** Coverage rate of confidence interval of CNN-BiLSTM model.

| Month | Confidence level | 4 hours | 24 hours | 72 hours |
|---|---|---|---|---|
| Jun | 97.5% | 100% | 97.91% | 97.57% |
| | 95% | 100% | 95.88% | 95.49% |
| | 90% | 94.12% | 94.84% | 93.10% |
| | 85% | 94.12% | 94.84% | 90.62% |

To verify the advantages of the non-parametric kernel density algorithm. As shown in the figure 20 and TABLE 14 in this study, the Gaussian Mixture Model (GMM) and Single Gaussian Model (SGM) are chosen to compare with the NPKDE. It can be seen that since the error distribution of wind power is not normal in the traditional sense its distribution number is irregular. The GMM and SGM need to define their distributions in advance, so although they can be quantified so that their forecasting are within the confidence interval, the accuracy is very poor, and they do not work properly in the real grid-connected power generation, which will consume a lot of economic costs to stabilize the wind power grid operation. The non-parametric kernel density estimation does not need to assume the distribution, and the accuracy is not only guaranteed to be within the confidence interval, but also to ensure the minimum area of the interval, which enables the grid to reduce certain costs to ensure the smooth operation of wind power grid connection.

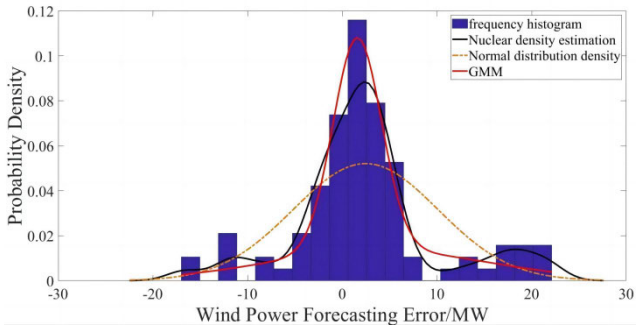


**FIGURE 20.** 4-hour wind power probabilistic forecasting results of Feb.

The application of confidence interval provide a feasible region for wind power dispatching and improve the dispatchable capability for wind farms and integrated energy systems.

**TABLE 14.** Confidence intervals of wind power forecasting errors under different distribution methods.

| Confidence level | GMM(MW) | SGM(MW) | NPKDE(MW) |
|---|---|---|---|
| 97.50% | 100% | 97.91% | 97.57% |
| 95% | 100% | 95.88% | 95.49% |
| 90% | 94.12% | 94.84% | 93.10% |
| 85% | 94.12% | 94.84% | 90.62% |

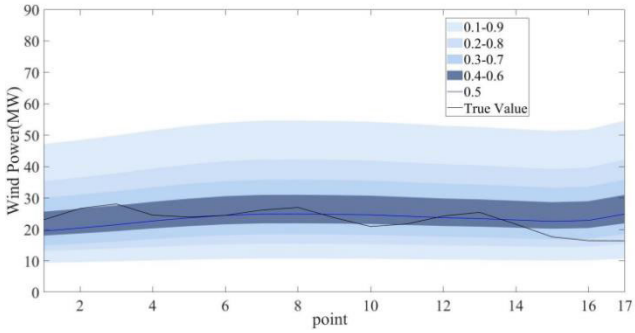


**FIGURE 21.** 4-hour wind power probabilistic forecasting results of Feb.

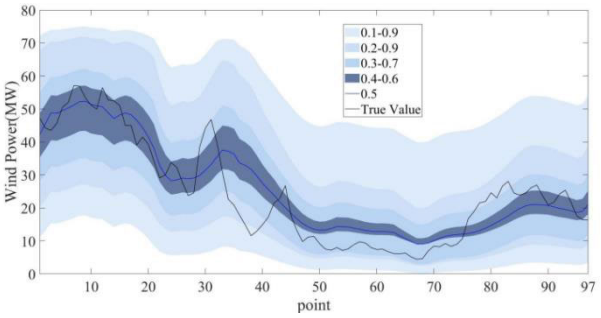


**FIGURE 22.** 24-hour wind power probabilistic forecasting results of Feb.

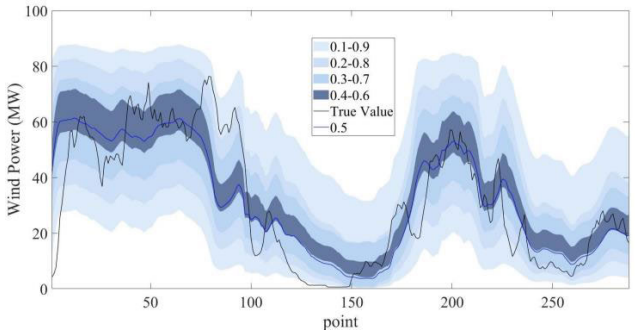


**FIGURE 23.** 72-hour wind power probabilistic forecasting results of Feb.

Meanwhile, the explicit interval can aid in determining the required reserve capacity in power grids as well as in improving the economic benefits of wind power generation.

To further explore the WOA-CNN-BiLSTM model WFPF and its uncertainty analysis, the authors also added probability forecasting results corresponding to the existing data. As shown in the Figs.21-23, which is the short-term

probability forecasting of wind power in the WOA-QRCNN-BILSTM algorithm. It can be seen that the probabilistic forecasting has certain advantages. It can accurately cover the true wind power in the 0.1-0.9 quartile range. However, although all data can be included within the 90% confidence interval, the interval range is 20% larger than the confidence interval established in this paper, making the required reserve capacity too large and without any economic benefits. Therefore, in practical use, the current technology cannot meet the requirements. But the WOA-CNN-BiLSTM-CM-NPKDE model can accurately and precisely characterize WFPF, providing better and safer technical support in actual uncertain optimization operations.

## VI. CONCLUSION

In the context of a significant integration of wind power into the grid, the demand for higher accuracy and reliability of WFPF at each operating point becomes more crucial. This study proposes a WOA-CNN-BiLSTM-CM-NPKDE based forecasting framework for WFPF and uncertainty analysis, aimed at supporting short-term multi-scale forecasting. To enhance the diversity of wind features in the models, the multi-scale pooling technique is adopted, and model optimization techniques are employed. The hybrid model achieves the extraction of feature links between continuous sequences and addresses issues related to missing information and long-term dependencies. Furthermore, the uncertainty analysis incorporates the Cloud model and NPKDE methods to determine the characteristics of WFPF and introduces three evaluation indices, refining and visualizing the WFPF uncertainty.

Insights obtained from the test case analysis include the following:

The CNN-BiLSTM model, owing to its time-recursive nature and feature extraction learning, demonstrates significant superiority over single models for WFPF. It is particularly suitable for analyzing wind power data with time-series characteristics, and compared to classical network models, the proposed model improves accuracy by 5.6%.

The adoption of WOA optimizes parameter settings, resulting in better performance and significantly improving the accuracy of the original model.

The proposed expectation, entropy, and hyper-entropy of the Cloud model facilitate qualitative description of the magnitude, fluctuation range, and concentration of fluctuation range of the WFPF amplitude. Additionally, the confidence interval of NPKDE provides a reliable forecasting range through quantitative analysis of WFPF uncertainty. These improvements collectively offer alternative forecasting options when optimizing the operational scheduling of wind power generation.

Future studies will focus on analyzing the law of forecasting uncertainty to enhance forecasting accuracy and model reliability. Also, further research will explore the application of the WOA-CNN-BiLSTM model in a complex spatial environment and the improvement of WFPF accuracy considering the type division of wind farms and multiple parameter optimization.

## REFERENCES

[1] F. Zhao, J. Lee, and A. Bath, "Global wind report 2021," Global Wind Energy Council, Brussels, Belgium, Tech. Rep., 2021. [Online]. Available: https://gwec.net/global-wind-report-2021/

[2] F. Zhang, P.-C. Li, L. Gao, Y.-Q. Liu, and X.-Y. Ren, "Application of autoregressive dynamic adaptive (ARDA) model in real-time wind power forecasting," *Renew. Energy*, vol. 169, pp. 129–143, May 2021, doi: 10.1016/j.renene.2021.01.003.

[3] I. Colak, S. Sagiroglu, and M. Yesilbudak, "Data mining and wind power prediction: A literature review," *Renew. Energy*, vol. 46, pp. 241–247, Oct. 2012, doi: 10.1016/j.renene.2012.02.015.

[4] J. Nielson, K. Bhaganagar, R. Meka, and A. Alaeddini, "Using atmospheric inputs for artificial neural networks to improve wind turbine power prediction," *Energy*, vol. 190, Jan. 2020, Art. no. 116273, doi: 10.1016/j.energy.2019.116273.

[5] Y. Sun, Z. Li, X. Yu, B. Li, and M. Yang, "Research on ultra-short-term wind power prediction considering source relevance," *IEEE Access*, vol. 8, pp. 147703–147710, 2020, doi: 10.1109/ACCESS.2020.3012306.

[6] D. Lee and R. Baldick, "Short-term wind power ensemble prediction based on Gaussian processes and neural networks," *IEEE Trans. Smart Grid*, vol. 5, no. 1, pp. 501–510, Jan. 2014, doi: 10.1109/TSG.2013.2280649.

[7] G. An, Z. Jiang, X. Cao, Y. Liang, Y. Zhao, Z. Li, W. Dong, and H. Sun, "Short-term wind power prediction based on particle swarm optimization-extreme learning machine model combined with AdaBoost algorithm," *IEEE Access*, vol. 9, pp. 94040–94052, 2021, doi: 10.1109/ACCESS.2021.3093646.

[8] Z. Sun and M. Zhao, "Short-term wind power forecasting based on VMD decomposition, ConvLSTM networks and error analysis," *IEEE Access*, vol. 8, pp. 134422–134434, 2020, doi: 10.1109/ACCESS.2020.3011060.

[9] B. Gu, T. Zhang, H. Meng, and J. Zhang, "Short-term forecasting and uncertainty analysis of wind power based on long short-term memory, cloud model and non-parametric kernel density estimation," *Renew. Energy*, vol. 164, pp. 687–708, Feb. 2021, doi: 10.1016/j.renene.2020.09.087.

[10] D. Y. Hong, T. Y. Ji, M. S. Li, and Q. H. Wu, "Ultra-short-term forecast of wind speed and wind power based on morphological high frequency filter and double similarity search algorithm," *Int. J. Electr. Power Energy Syst.*, vol. 104, pp. 868–879, Jan. 2019, doi: 10.1016/j.ijepes.2018.07.061.

[11] S. V. Medina and U. P. Ajenjo, "Performance improvement of artificial neural network model in short-term forecasting of wind farm power output," *J. Mod. Power Syst. Clean Energy*, vol. 8, no. 3, pp. 484–490, May 2020, doi: 10.35833/mpce.2018.000792.

[12] X. Dong, Y. Sun, Y. Li, X. Wang, and T. Pu, "Spatio-temporal convolutional network based power forecasting of multiple wind farms," *J. Mod. Power Syst. Clean Energy*, vol. 10, no. 2, pp. 388–398, Mar. 2022, doi: 10.35833/Mpce.2020.000849.

[13] R. Yuan, B. Wang, Z. Mao, and J. Watada, "Multi-objective wind power scenario forecasting based on PG-GAN," *Energy*, vol. 226, Jul. 2021, Art. no. 120379, doi: 10.1016/j.energy.2021.120379.

[14] T. Zhang, Y. Huang, H. Liao, and Y. Liang, "A hybrid electric vehicle load classification and forecasting approach based on GBDT algorithm and temporal convolutional network," *Appl. Energy*, vol. 351, Dec. 2023, Art. no. 121768, doi: 10.1016/j.apenergy.2023.121768.

[15] X. Fang and M. Cui, "Analytical model of day-ahead and real-time price correlation in strategic wind power offering," *J. Mod. Power Syst. Clean Energy*, vol. 8, no. 5, pp. 1024–1027, Sep. 2020, doi: 10.35833/MPCE.2019.000598.

[16] M. Xu, Z. Lu, Y. Qiao, and Y. Min, "Modelling of wind power forecasting errors based on kernel recursive least-squares method," *J. Mod. Power Syst. Clean Energy*, vol. 5, no. 5, pp. 735–745, Sep. 2017, doi: 10.1007/s40565-016-0259-7.

[17] M. S. H. Lipu, Md. S. Miah, M. A. Hannan, A. Hussain, M. R. Sarker, A. Ayob, M. H. M. Saad, and Md. S. Mahmud, "Artificial intelligence based hybrid forecasting approaches for wind power generation: Progress, challenges and prospects," *IEEE Access*, vol. 9, pp. 102460–102489, 2021, doi: 10.1109/ACCESS.2021.3097102.

[18] C. Miao, H. Li, X. Wang, and H. Li, "Ultra-short-term prediction of wind power based on sample similarity analysis," *IEEE Access*, vol. 9, pp. 72730–72742, 2021, doi: 10.1109/ACCESS.2021.3080140.

[19] L. Tan, J. Han, and H. Zhang, "Ultra-short-term wind power prediction by Salp swarm algorithm-based optimizing extreme learning machine," *IEEE Access*, vol. 8, pp. 44470–44484, 2020, doi: 10.1109/Access.2020.2978098.
[20] J. M. González-Sopeña, V. Pakrashi, and B. Ghosh, "Multi-step ahead wind power forecasting for Ireland using an ensemble of VMD-ELM models," in *Proc. 31st Irish Signals Syst. Conf.*, 2020, pp. 187–191.
[21] Q. Tu, S. Miao, F. Yao, Y. Li, H. Yin, J. Han, D. Zhang, and W. Yang, "Forecasting scenario generation for multiple wind farms considering time-series characteristics and spatial–temporal correlation," *J. Mod. Power Syst. Clean Energy*, vol. 9, no. 4, pp. 837–848, Jul. 2021, doi: 10.35833/MPCE.2020.000935.
[22] M. A. Hossain, R. K. Chakrabortty, S. Elsawah, and M. J. Ryan, "Very short-term forecasting of wind power generation using hybrid deep learning model," *J. Cleaner Prod.*, vol. 296, May 2021, Art. no. 126564, doi: 10.1016/j.jclepro.2021.126564.
[23] H.-Z. Wang, G.-Q. Li, G.-B. Wang, J.-C. Peng, H. Jiang, and Y.-T. Liu, "Deep learning based ensemble approach for probabilistic wind power forecasting," *Appl. Energy*, vol. 188, pp. 56–70, Feb. 2017, doi: 10.1016/j.apenergy.2016.11.111.
[24] L. Ye, C. Zhang, Y. Tang, W. Zhong, Y. Zhao, P. Lu, B. Zhai, H. Lan, and Z. Li, "Hierarchical model predictive control strategy based on dynamic active power dispatch for wind power cluster integration," *IEEE Trans. Power Syst.*, vol. 34, no. 6, pp. 4617–4629, Nov. 2019.
[25] J. Yan, Y. Liu, S. Han, Y. Wang, and S. Feng, "Reviews on uncertainty analysis of wind power forecasting," *Renew. Sustain. Energy Rev.*, vol. 52, pp. 1322–1330, Dec. 2015, doi: 10.1016/j.rser.2015.07.197.
[26] Y. Wang, Q. Hu, D. Srinivasan, and Z. Wang, "Wind power curve modeling and wind power forecasting with inconsistent data," *IEEE Trans. Sustain. Energy*, vol. 10, no. 1, pp. 16–25, Jan. 2019, doi: 10.1109/TSTE.2018.2820198.
[27] H. Zhang, Y. Liu, J. Yan, S. Han, L. Li, and Q. Long, "Improved deep mixture density network for regional wind power probabilistic forecasting," *IEEE Trans. Power Syst.*, vol. 35, no. 4, pp. 2549–2560, Jul. 2020, doi: 10.1109/TPWRS.2020.2971607.
[28] Z. Jinhua, Y. Jie, W. Wenjing, and L. Yongqian, "Research on short-term forecasting and uncertainty of wind turbine power based on relevance vector machine," *Energy Proc.*, vol. 158, pp. 229–236, Feb. 2019, doi: 10.1016/j.egypro.2019.01.081.
[29] W. Dong, H. Sun, J. Tan, Z. Li, J. Zhang, and H. Yang, "Regional wind power probabilistic forecasting based on an improved kernel density estimation, regular vine copulas, and ensemble learning," *Energy*, vol. 238, Jan. 2022, Art. no. 122045, doi: 10.1016/j.energy.2021.122045.
[30] W. Song, H. Liu, and E. Zio, "Long-range dependence and heavy tail characteristics for remaining useful life prediction in rolling bearing degradation," *Appl. Math. Model.*, vol. 102, pp. 268–284, Feb. 2022, doi: 10.1016/j.apm.2021.09.041.
[31] W. Wei, J. Wu, Y. Yu, T. Niu, and X. Deng, "Uncertainty quantification analysis of wind power: A data-driven monitoring-forecasting framework," *IEEE Access*, vol. 9, pp. 84403–84416, 2021, doi: 10.1109/ACCESS.2021.3086583.
[32] G. Qin, M. Zhang, Q. Yan, C. Xu, and D. M. Kammen, "Comprehensive evaluation of regional energy internet using a fuzzy analytic hierarchy process based on cloud model: A case in China," *Energy*, vol. 228, Aug. 2021, Art. no. 120569, doi: 10.1016/j.energy.2021.120569.
[33] L. Xiao, G. Huang, and G. Zhang, "Improved assessment model for candidate design schemes with an interval rough integrated cloud model under uncertain group environment," *Eng. Appl. Artif. Intell.*, vol. 104, Sep. 2021, Art. no. 104352, doi: 10.1016/j.engappai.2021.104352.
[34] H. Shin, H. R. Roth, M. Gao, Le Lu, Z. Xu, I. Nogues, J. Yao, D. Mollura, and R. M. Summers, "Deep convolutional neural networks for computer-aided detection: CNN architectures, dataset characteristics and transfer learning," *IEEE Trans. Med. Imag.*, vol. 35, no. 5, pp. 1285–1298, May 2016, doi: 10.1109/TMI.2016.2528162.
[35] Y.-M. Zhang and H. Wang, "Multi-head attention-based probabilistic CNN-BiLSTM for day-ahead wind speed forecasting," *Energy*, vol. 278, Sep. 2023, Art. no. 127865, doi: 10.1016/j.energy.2023.127865.

**TIANREN ZHANG** received the master's degree from the North China University of Water Resources and Electric Power, in 2021. He is currently pursuing the Ph.D. degree in energy engineering with the University of Science and Technology of China. He is a Research Assistant with the Guangzhou Energy Research Institute, CAS, China. He has published seven articles in academic journals. His research interests include forecasting, data analysis, intelligent computing, multi-energy optimization scheduling, and smart grids.

**YUPING HUANG** (Member, IEEE) received the master's degree in industrial engineering from West Virginia University, USA, in 2011, and the Ph.D. degree in industrial engineering from the University of Central Florida, USA, in 2014. From 2015 to 2017, she was a Postdoctoral Associate with the University of Central Florida. Since 2017, she has been a Researcher with the Guangzhou Institute of Energy Conversion, CAS, China, and a Doctoral Supervisor of energy system management with the School of Energy Science and Engineering, University of Science and Technology of China. She is the Principal Investigator of multiple national, provincial, ministerial, and international collaborative projects. Her contributions are evidenced by over 20 articles published in SCI/EI academic journals and 12 authorized patents. Her research interests include intelligent energy management systems, vehicle-to-grid system operation, optimization modeling, and artificial intelligence application in the decision-making for complex energy systems. She was a recipient of the IEEE PES Best Paper Award.

**HUI LIAO** received the master's degree from Zhejiang University, in 2012. He is currently pursuing the Ph.D. degree in energy engineering with the Chinese Academy of Sciences. He is an Engineer with the Guangzhou Institute of Energy Research, CAS, China. He has authorized ten patents and published five journal articles. His research interests include multi-energy optimization scheduling and smart grids.

**XIANFU GONG** received the master's degree in electric power engineering from Zhejiang University, in 2012. He is currently a Senior Engineer with the Guangdong Provincial Planning Center, China Southern Power Grid Company Ltd. He has published three articles in SCI journals. His research interests include energy planning, energy forecasting, and multi-energy optimal scheduling direction.

**BO PENG** received the master's degree in electric power engineering from Zhejiang University, in 2017. He is currently an Engineer with the Guangdong Provincial Planning Center, China Southern Power Grid Company Ltd. He has published over ten articles in the SCI journals. His research interests include energy planning, energy data analysis, and multi-energy forecasting.